Fracture Prediction for Crashworthiness Assessment of Aluminum Bumper Systems

Christian Leppin[1], Matthias Kutscher[2], Martin Feuerstein[2], Gernot Oberhofer[3]

[1] Alcan Technology & Management, Neuhausen, Switzerland
[2] Alcan Singen GmbH, Gottmadingen, Germany
[3] Matfem Partnerschaft Dr. Gese & Oberhofer, Munich, Germany

Abstract:

Alcan relies strongly on crashworthiness simulations in its development of light weight automotive crash management systems at Gottmadingen, Germany. The effectiveness of CAE-based crash performance assessments considerably depends on the ability of the numerical model to predict the actual material behavior including fracture. In this paper, the user material model *MF GenYld + CrachFEM* coupled with *LS-Dyna* is used to model the fracture behavior of an EN-AW 6082 T6 aluminum extrusion alloy used for aluminum bumper cross-members. The model parameters are identified in a comprehensive testing program. Based on a 3-point bending validation test of a bumper profile, the performance of the material model and the influence of the element formulation are investigated.

Keywords:

Crashworthiness simulation, fracture prediction, aluminum extrusions, automotive crash management.

1   Introduction

The freedom in geometrical design along with the excellent energy absorption and general light weight properties of aluminum make high strength aluminum extrusions to a very effective material for light weight crash management components. As an automotive supplier of aluminum bumper systems (front and rear) and impact beams, Alcan at Gottmadingen, Germany strongly relies on crashworthiness simulations for feasibility studies and optimization of the design in the product development process. For a proper CAE-based crash performance assessment of the design, appropriate constitutive models for the deformation and failure behavior of the material are important.

In this paper, a full mechanical characterization of an EN-AW 6082 T6 aluminum extrusion alloy is presented. A comprehensive experimental program was performed to identify the anisotropic material behavior including fracture and for modeling with the commercial material model software package *MF GenYld + CrachFEM*. The module *MF GenYld* within this software package offers a variety of hardening models and yield locus formulations, e.g. Hill 1948, Hill 1990, Barlat 2000 and Dell 2006. The module *CrachFEM* describes failure due to local necking (for shell elements only) as well as ductile normal fracture and ductile shear fracture (for shell and solid elements). The software package may be coupled as a user material model to *LS-Dyna* and other explicit FEM programs.

The material model is validated by a 3-point bending test of the extrusion profile investigated in this study. In order to provoke failure, the experimental setup is designed to load the component far beyond the level for which it originally was designed.

2   Material characterization

2.1   Plastic deformation model

Tensile test results in extrusion direction in combination with layered compression test results are used to identify the reference hardening curve of the EN-AW 6082 T6 aluminum extrusion material. Several empirical hardening laws have been fitted to the experimental data with best results for the Hocket-Sherby approximation[*]:

$$\sigma = a - (a - \sigma_0) \cdot \exp(-c \cdot \varepsilon_{eq}^n) \qquad (1)$$

with the following parameters: a = 425.9 MPa, σ_0 = 328.4 MPa, c = 12.1099 and n = 1.0725 .
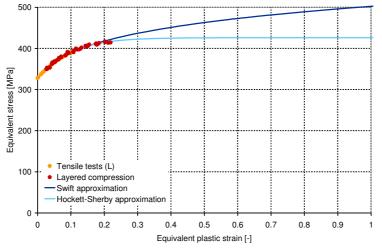

Figure 1: Hardening of the EN-AW 6082 T6 aluminum extrusion – tensile tests in extrusion direction, layered compression tests and approximations with the Swift and the Hockett-Sherby hardening laws

[*] Mechanical properties: $R_{p0.2}$=330MPa, R_m=360MPa, A_{50}=15%. Previous dynamic tests with strain-rates up to 250 s^{-1} have not revealed any noticeable strain-rate dependency of the alloy with respect to material strength. Therefore, strain rate effects are not considered in the plastic deformation model.

Due to its strongly oriented fibrous microstructure the extrusion alloy exhibits a quite pronounced plastic anisotropy. Several yield locus formulations have been fitted to the results of tensile tests in 0°, 45° and 90° with respect to extrusion direction, layered compression tests and in plane torsion tests. The orthotropic yield locus formulation of Dell 2006 (see appendix, respectively [1] for details) was identified as the best formulation for the profile EN-AW 6082 T6 with the following coefficients:

m_1 = 32 m_2 = 4 c = 0.6
c_1 = 1.0841 c_2 = 1.1916 c_3 = 0.9561 c_4 = 1.1332
d_1 = 0.7774 d_2 = 0.8965 d_3 = 1.0038 d_4 = 1.0166

The out-of-plane coefficients were set to one: $c_5 = c_6 = d_5 = d_6 = 1$. The yield locus according to Dell 2006 can be used in case of plane stress condition (shell discretization) as well as general 3d stress state (solid discretization).
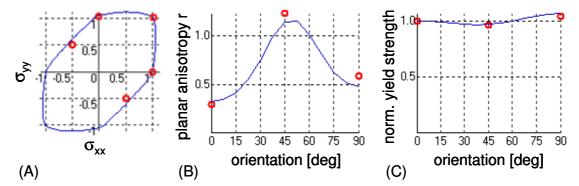

Figure 2: Yield locus (A) and direction dependence of planar anisotropy (B) and normalized uniaxial tensile yield stress (C) of the EN-AW 6082 T6 aluminum extrusion for a plastic strain of 0.05 showing the approximation with the Dell 2006 criterion in comparison with the experiments

2.2   Crach failure model

The failure prediction module *CrachFEM* differentiates three types of failure initiation: localized necking, ductile normal fracture due to void nucleation, void growth and void coalescence, and shear fracture due to shear band localization.

The criterion for localized necking is only used for shell discretizations, as shells are not able to resolve a localized neck. Along the lines of the original idea by Marciniak and Kuczynski [2], a perturbation method in combination with an orthotropic material model is utilized to predict the initiation of necking failure due to membrane instability (algorithm Crach). One of the basic ideas of the model is an improved geometrical representation of the initial imperfection. Furthermore, strain rate dependent hardening behavior is taken into consideration, orthotropic plasticity is included, and an isotropic-kinematic hardening model is used to account for non-linear strain paths. The initial imperfection of the material is calibrated based on the limit strain for necking in one test. See [3] for details on the algorithm. The necessary input for the algorithm Crach is the hardening behavior, the strain rate sensitivity and the Lankford coefficients of the material.

As a ductile normal fracture criterion, the equivalent fracture strain for any given constant temperature is assumed to be a function of a stress state parameter β which is a function of the stress triaxiality η and the ratio of first principal stress σ_1 to the v. Mises equivalent stress σ_M:

$$\beta = f\left(\frac{\sigma_1}{\sigma_M}, \eta\right) = \frac{1 - s_{NF} \cdot \eta}{(\sigma_1/\sigma_M)} = \frac{\sigma_M - s_{NF} \cdot (\sigma_1 + \sigma_2 + \sigma_3)}{\sigma_1} \quad . \tag{2}$$

Here, s_{NF} is a material dependent parameter and normal fracture can occur only if the first principal strain σ_1 is positive. The normal fracture curve is described by the empirical function

$$\varepsilon_{eq}^{**} = d \cdot e^{q \cdot \beta} \tag{3}$$

with two material coefficients d and q.

As a ductile shear fracture criterion, the equivalent fracture stain is assumed to be a function of the shear stress parameter θ which is defined as:

$$\theta = \frac{1 - k_{SF} \cdot \eta}{\phi} \qquad (4)$$

Here, k_{SF} is a material parameter describing the influence of the stress triaxiality η on shear fracture and ϕ is the ratio of the maximum shear stress to the v. Mises equivalent stress σ_M:

$$\phi = \frac{\tau_{max}}{\sigma_M} \qquad \text{where} \qquad \tau_{max} = \frac{\sigma_1 - \sigma_3}{2} \qquad . \qquad (5)$$

The shear fracture curve $\varepsilon_{eq}^{**}(\theta)$ is given by the following empirical function:

$$\varepsilon_{eq}^{**} = \frac{\varepsilon_{SF}^{+} \sinh\left(f\left(\theta - \theta^{-}\right)\right) + \varepsilon_{SF}^{-} \sinh\left(f\left(\theta^{+} - \theta\right)\right)}{\sinh\left(f\left(\theta^{+} - \theta^{-}\right)\right)} \qquad (6)$$

with the parameters:

$\theta^{+} = 2 \cdot (1 - 2 \cdot k_{SF})$ shear stress parameter at equibiaxial tension
$\theta^{-} = 2 \cdot (1 + 2 \cdot k_{SF})$ shear stress parameter at equibiaxial compression
ε_{SF}^{+} fracture strain at equibiaxial tension
ε_{SF}^{-} fracture strain at equibiaxial compression
f material parameter

The material parameters ε_{SF}^{+}, ε_{SF}^{-} and f may depend on the strain-rate. Note, that the representation for normal fracture and the representation for shear fracture are both applicable to general 3-dimensional stress states, see [4] for details.

The fracture parameters are determined by the following experiments: tensile test, tensile test with circular hole and 3-point bending test (all tests in 0°, 45° as well as in 90° with respect to extrusion direction). Moreover, notched tensile test, Erichsen test, grooved shear test, compression test, tensile test with 45°, respectively 90° groove (all tests in extrusion direction only). Based on the results of these tests, the material parameters for ductile normal fracture in equation (2) and (3) were determined as:

$s = 0.2390$ $d = 0.1020$ $q = 2.1898$

Furthermore, by optimization, the shear fracture parameter k_{SF} in (4) was identified as:

$k_{SF} = 0.1$

With this parameter, the shear fracture curve (6) is defined by the following parameters:

$\varepsilon_{SF}^{+} = 0.41$ $\varepsilon_{SF}^{-} = 2.67$ $f = 2.62$
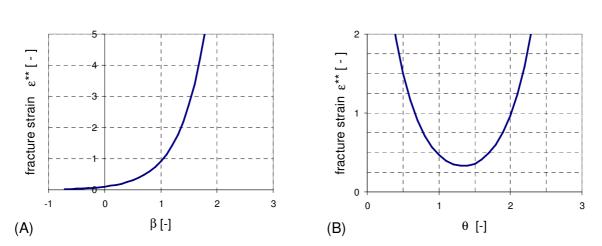

(A)   (B)

Figure 3: Quasi-static normal fracture curve $\varepsilon^{**}(\beta)$ *and shear fracture curve* $\varepsilon^{**}(\theta)$ *of the EN-AW 6082 T6 extrusion profile*

The fracture limit curves for ductile normal fracture and ductile shear fracture are given in Figure 3 (A), respectively Figure 3 (B). Figure 4 gives all failure limits (including forming limit curve for localized necking) in one diagram for the special case of plane stress condition.
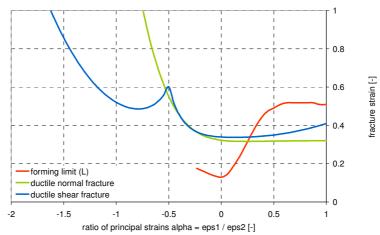

Figure 4: Ductile normal fracture, ductile shear fracture and forming limit due to membrane instability of the extrusion EN-AW 6082 T6 plotted as fracture or failure strain as a function of the ratio of principal strain rates for the special case of plane-stress conditions

2.3   Homogeneity of properties

Due to the production process the mechanical property distribution in aluminum extrusion profiles typically is less homogeneous than in sheet material. The inhomogeneity of properties of the profile in this investigation was quantified by selected tests of material taken form all different thickness wall sections. Neither the hardening behavior, nor the fracture behavior turned out to be significantly inhomogeneous. Therefore, quasi-homogenous properties are assumed for the finite element simulation.

3   Validation test

Three quasi-static 3-point bending tests have been performed to validate the fracture model for extruded EN-AW 6082 T6 bumper profiles, see experimental setup in Figure 5. – As mentioned in the introduction, the experiment is designed to load the component far beyond the level for which it originally has been designed in order to provoke failure. – The punch force and displacement have been recorded over time. Furthermore, a stochastic pattern was applied in the central area of the test profiles and during each test the deformations in this area have been measured with the stereo optical strain measuring system Aramis.
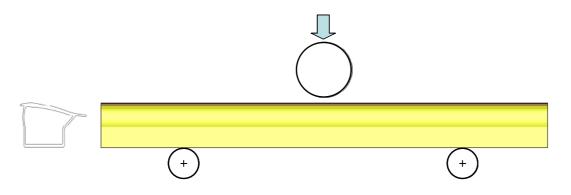

Figure 5: 3-point bending test used to validate the fracture model for the bumper profiles

4   Finite element model

The validation test is simulated with two different discretizations: To begin with, a standard shell element discretization with underintegrated 4-node Belytschko-Tsay elements is used (*LS-Dyna* shell element formulation 2), see Figure 6. In addition, a solid element discretization with underintegrated 8-node hexahedron elements is investigated (*LS-Dyna* solid element formulation 1), as the shell element discretization may have shortcomings in the areas of wall intersections with mass concentrations, see Figure 7. A total of 885'000 elements were used to ensure proper aspect ratios of the elements and a minimum number of 3 elements across the wall thickness, which actually is comparatively coarse depending on the mode of loading. A too stiff behavior of the component is expected as a result and additional mesh refinement most likely will lead to a different result. Due to the model size a convergence study has not been performed however.

Regarding the time discretization, the entire deformation process is scaled to a total simulation time of 60ms. No mass scaling has been used for the shell element model, while for the solid element model a mass scaling of 50% has been used in order to achieve a minimum time step of 2.0e-4 ms.
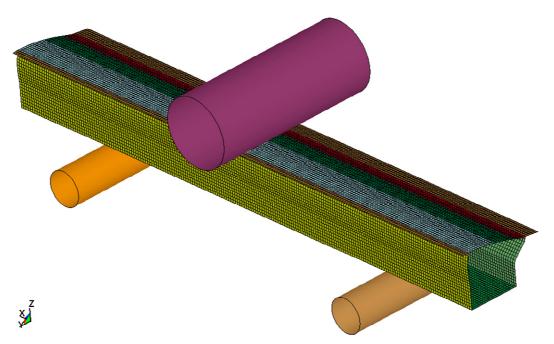

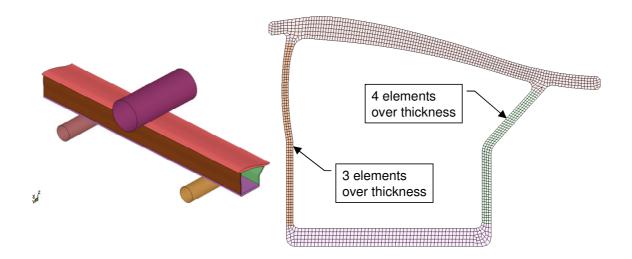*Figure 6: Finite element discretization of the 3-point bending test with shell elements*

Figure 7: Finite element discretization of the 3-point bending test with solid elements

5   Results and discussion

In a first set of three simulations with the shell element model, the modular concept of *MF GenYld + CrachFEM* was exploited to explore the influence of the yield locus and the failure model with the following different combinations:
-        standard v. Mises yield locus, no failure considered (*LS-Dyna* Mat 24)
-        standard v. Mises yield locus (*MF-GenYld*) in combination with the CrachFEM failure model
-        Dell 2006 orthotropic yield locus (*MF-GenYld*) in combination with the CrachFEM failure model

For both simulations with the CrachFEM failure model, the failure parameters reported in section 2.2 are used. A standard 5 point Labatto integration rule is used in shell thickness direction.

Figure 8 shows the comparison of the force vs. displacement curves of these simulations with different material models and the experimental test results.[†] At the initial force maximum all curves are well in agreement with the test results. With increasing displacement however, the standard v. Mises material model without failure (*LS-Dyna* Mat 24) considerably overpredicts the force level, especially beyond the second force maximum. Both curves of the simulations utilizing the CrachFEM failure model perform significantly better. The force level is still overpredicted in the neighborhood of the second force maximum, but the numerical results are much closer to the test results. Since the two curves are very close to each other, in this case material failure obviously is the dominant influence and ignoring the actual strongly anisotropic behavior of the extrusion profile only has a minor effect on the global force level.
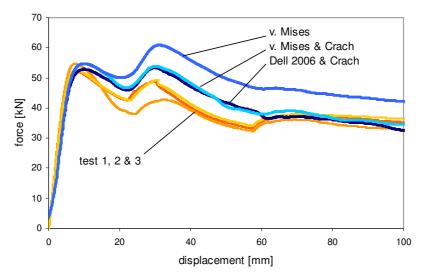

Figure 8: Comparison of the force vs. displacement curves of the experimental test results and simulations with shell elements using different material models.

As mentioned in the previous comparison of material models, the standard model with shell element and 5 point Lobatto integration rule gives a quite reasonable correlation between simulation and experiment with respect to force-displacement behavior. Likewise, the strain measurements with the Aramis optical system show that the location and time of fracture initiation are very well predicted (see Figure 10). The initial maximum in the force-displacement curve is slightly underestimated, which very likely is a consequence of the rather poor description of the mass concentrations at the wall intersections with shell elements. After buckling has started, this influence decreases and the force-displacement curve is calculated with good accuracy. With an increase of the number of integration points from 5 to 7, the correlation at higher degree of deformation is further improved. However the value of the initial force peak is predicted even lower than with 5 integration points.

[†] All FEA-based force vs. displacement curves in this paper are filtered in LS-PrePost using a cosines filter with a frequency of 180 Hz in order to suppress small oscillations caused by inertia effects. Besides suppressing these small oscillations the influence of the filtering procedure onto the force deflection curves is neglegible.

As expected the solid discretization leads to a slightly too stiff deformation behavior of the component. This very likely is due to the coarse mesh with only 3 elements, i.e. 3 integration points over the thickness in the critical areas which undergo bending. Since the integration points are in the middle of the elements and not on the surface and since the discretization with only 3 elements through thickness generally is too stiff, the local deformations in areas of wall buckling are predicted too small as a consequence. As a result the failure risks are also underestimated and the solid model predicts the initiation of failure too late, see comparison of failure risk in Figure 11.
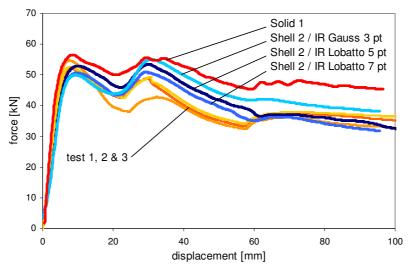

Figure 9: Comparison of the force vs. displacement curves of the experimental test results and simulations with different element formulations.

Aramis measurements   **CrachFEM failure prediction**
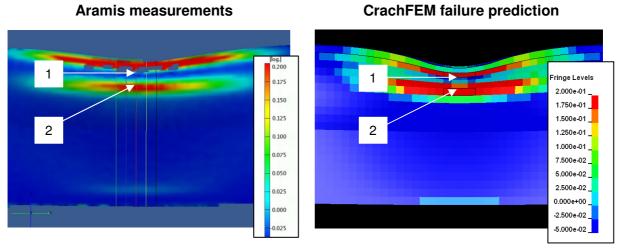

Figure 10: Maximum principal strain at the outer surface after initiation of fracture – Aramis optical strain measurements (left) and simulation with shell discretization and MF GenYld + CrachFEM (right)

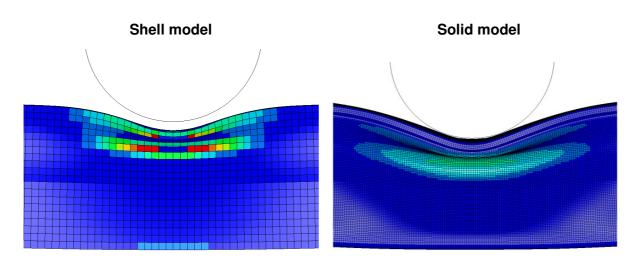**Shell model**   **Solid model**

Figure 11: Comparison of the maximum failure risk distribution briefly after fracture initiation – correct prediction with shell model (left) still subcritical risk of fracture in solid model (right)

6   Conclusions

A comprehensive characterization of an EN-AW 6082 T6 aluminum extrusion has been completed. The simulation of a 3-point bending test with the user material model *MF GenYld + CrachFEM* shows good correlation with the experiment. Especially crack initiation is very accurately described. The investigation revealed that in this test the failure model is the deciding factor for good results. No major differences have been observed in global force level when the yield locus model was switched from the complex orthotropic Dell 2006 model to a simple v. Mises model while maintaining an active fracture model. This observation certainly can not be generalized to other load cases. As has been shown in previous publications, the yield locus can also influence the local strain distribution and as a consequence the failure initiation.

The choice of different element formulations, respectively integration rules has a major influence on the results. Good results where obtained with standard shell elements and standard 5 point Labatto integration rule. Nevertheless an increase of the number of integration points to 7 revealed the deficiencies of shell elements regarding adequate representation of mass concentrations at wall intersections of extrusion profiles. The investigation demonstrates that this issue cannot be solved with a solid discretization, since buckling of the wall sections cannot be modeled properly with a mesh with reasonably sized elements due to the detrimental effect on time step and total number of elements. The use of thick shells (TSHELL) in *LS-Dyna* might be a compromise which should be validated in the future. The yield locus model of Dell 2006 and the fracture models for ductile normal fracture and ductile shear fracture in CrachFEM can be used throughout all discretization levels.

Finally, a further source for deficiencies not discussed in this paper so far, most likely is the rather crude modeling of crack propagation by simple element deletion. Though widely used, this approach does not account for the singularity at the crack tip and other mechanisms driving crack growth, and, even worse, might lead to strongly mesh dependent results.

7   References

[1]   Dell H., Gese H., Oberhofer, G.: "Advanced Yield Loci and Anisotropic Hardening in the Material Model MF GENYLD + CRACHFEM", in Proceedings of Numisheet 2008, September 1-5, Interlaken, Switzerland

[2]   Marciniak Z. and Kuczynski K.: "Limit strains in the processes of stretch-forming sheet metal", Int. J. of Mechanical Sciences 9, 1967, pp. 609-620.

[3]   Gese H. and Dell H.: "Numerical Prediction of FLC with the Program CRACH", Proceedings of FLC Zurich 2006, 15th – 16th March 2006, IVP, ETH Zurich, Switzerland

[4]   H. Dell, H. Gese, G. Oberhofer: CrachFEM – A Comprehensive Approach for the Prediction of Sheet Metal Failure. Numiform '07. American Institute of Physics, 2007, pp 165–170.

8   Appendix

The yield locus Dell (2006) is described by:

$$\sigma_{eq} = k_1 \cdot \left(\left| X_1 - X_2 \right|^{m_1} + \left| X_2 - X_3 \right|^{m_1} + \left| X_3 - X_1 \right|^{m_1} \right)^{1/m_1}$$

$$+ k_2 \cdot \left(\left| Y_1 \right|^{m_2} + \left| Y_2 \right|^{m_2} + \left| Y_3 \right|^{m_2} \right)^{1/m_2}$$

(7)

Here, X_1, X_2 and X_3 are the principal components of the vector $\mathbf{X}$ which may be calculated from the stress tensor $\boldsymbol{\sigma}$ with a matrix $\mathbf{C}$ as follows:

$$\begin{pmatrix} X_x \\ X_y \\ X_z \\ X_{xy} \\ X_{yz} \\ X_{zx} \end{pmatrix} = \frac{1}{3} \cdot \begin{bmatrix} c_2 + c_3 & -c_3 & -c_2 & 0 & 0 & 0 \\ -c_3 & c_3 + c_1 & -c_1 & 0 & 0 & 0 \\ -c_2 & -c_1 & c_1 + c_2 & 0 & 0 & 0 \\ 0 & 0 & 0 & 3 \cdot c_4 & 0 & 0 \\ 0 & 0 & 0 & 0 & 3 \cdot c_5 & 0 \\ 0 & 0 & 0 & 0 & 0 & 3 \cdot c_6 \end{bmatrix} \cdot \begin{pmatrix} \sigma_x \\ \sigma_y \\ \sigma_z \\ \sigma_{xy} \\ \sigma_{yz} \\ \sigma_{zx} \end{pmatrix}$$

(8)

Likewise, Y_1, Y_2 and Y_3 are the principal componets of the vector $\mathbf{Y}$, which can be determined by means of a matrix $\mathbf{D}$:

$$\begin{pmatrix} Y_x \\ Y_y \\ Y_z \\ Y_{xy} \\ Y_{yz} \\ Y_{zx} \end{pmatrix} = \frac{1}{3} \cdot \begin{bmatrix} d_2 + d_3 & -d_3 & -d_2 & 0 & 0 & 0 \\ -d_3 & d_3 + d_1 & -d_1 & 0 & 0 & 0 \\ -d_2 & -d_1 & d_1 + d_2 & 0 & 0 & 0 \\ 0 & 0 & 0 & 3 \cdot d_4 & 0 & 0 \\ 0 & 0 & 0 & 0 & 3 \cdot d_5 & 0 \\ 0 & 0 & 0 & 0 & 0 & 3 \cdot d_6 \end{bmatrix} \cdot \begin{pmatrix} \sigma_x \\ \sigma_y \\ \sigma_z \\ \sigma_{xy} \\ \sigma_{yz} \\ \sigma_{zx} \end{pmatrix}$$

(9)

The coefficients k_1 and k_2 are determined from the yield locus parameters:

$$k_1 = 3 \cdot c \cdot \left(\left| c_2 + 2 \cdot c_3 \right|^{m_1} + \left| c_2 - c_3 \right|^{m_1} + \left| 2 \cdot c_2 + c_3 \right|^{m_1} \right)^{-1/m_1}$$

$$k_2 = 3 \cdot (1 - c) \cdot \left(\left| d_2 + d_3 \right|^{m_2} + \left| d_2 \right|^{m_2} + \left| d_3 \right|^{m_2} \right)^{-1/m2}$$

(10)

The exponents m_1 and m_2 must be positive, but are not limited to natural numbers. The coefficient c with $0 \leq c \leq 1$ is a weight for the two sub-formulations described by the coefficients m_1 and $c_{1,...,6}$ and the coefficients m_2 and $d_{1,...,6}$ respectively.

For plane-stress states, the matrices $\mathbf{C}$ and $\mathbf{D}$ are reduced to:

$$\mathbf{C} = \frac{1}{3} \cdot \begin{bmatrix} c_2 + c_3 & -c_3 & 0 \\ -c_3 & c_3 + c_1 & 0 \\ 0 & 0 & 3 \cdot c_4 \end{bmatrix} \qquad \mathbf{D} = \frac{1}{3} \cdot \begin{bmatrix} d_2 + d_3 & -d_3 & 0 \\ -d_3 & d_3 + d_1 & 0 \\ 0 & 0 & 3 \cdot d_4 \end{bmatrix}$$

(11)

The formulation requires fifteen coefficients for the general stress state:

$m_1, m_2, c, c_{1,...,6}, d_{1,...,6}$

For the plane-stress state, eleven independent coefficients are needed:

$m_1, m_2, c, c_{1,...,4}, d_{1,...,4}$ $c_5 = c_6 = 0$ $d_5 = d_6 = 0$